Applied Thermal Engineering 252 (2024) 123687

Contents lists available at ScienceDirect

Applied Thermal Engineering

journal homepage: www.elsevier.com/locate/apthermeng

Research Paper

Characterizing thermal runaway of reservoir rocks under electromagnetic irradiation towards hydrogen generation from petroleum reservoirs

Baizheng An [a], Keju Yan [a], Brandon Robinson [b], Jianli Hu [b], Qingwang Yuan [a,*]

[a] Bob L. Herd Department of Petroleum Engineering, Texas Tech University, 2500 Broadway, Lubbock, TX 79409, USA
[b] Department of Chemical and Biomedical Engineering, West Virginia University, Morgantown, WV 26506, USA

ARTICLE INFO

Keywords:
Thermal runaway
Reservoir rocks
Electromagnetic heating
Minerals
Hydrogen production

ABSTRACT

Electromagnetic(EM)-assisted catalytic heating presents a novel method for in-situ hydrogen production from petroleum reservoirs. This study delves into the interaction between electromagnetic waves and reservoir rocks, characterizing the fundamentals behind thermal runaway (TR) phenomenon in sandstones and shales. Utilizing a custom microwave reactor and advanced analysis techniques, we identify the microwave-induced thermal runaway phenomenon in San Saba sandstone rocks at ~ 568 °C and Mancos shale rocks at ~ 253 °C, emphasizing the role of mineral, elemental compositions, and dielectric properties in these differences. We also identified that chlorite, albite, and illite are major contributors to thermal runaway and the significant reduction in power required for reheating rocks, saving 50.0–66.7% for sandstone and 64.0–80.0% for shale. This work contributes new insights into the occurrence and mechanisms of thermal runaway in reservoir rocks, therefore providing an efficient way for enhancing heating efficiency and reducing energy input for in-situ hydrogen production. This research further de-risks the emerging technology for in-situ hydrogen production from petroleum reservoirs via electromagnetic-assisted catalytic heating.

1. Introduction

To cope with the increasing global challenge of climate change and meet the goals of the Paris Agreement, a series of strategies have been developed to reduce greenhouse gas emissions and transform fossil fuels into cleaner energy. Particularly, the petroleum industry is actively engaged in the transition towards sustainable and low-carbon energy sources in order to achieve the net-zero emissions by 2050[1,2]. One approach to decarbonize the petroleum industry is to convert oil and gas into hydrogen (H_2). As of 2019, about 95% of hydrogen is produced by steam methane reforming (SMR) in the United States, with a carbon footprint of 9–10 kg CO_2/kg H_2 involved[3]. The carbon capture, utilization, and storage (CCUS) is therefore required to mitigate the carbon footprint. However, CCUS is costly and needs significant investments from government and private sectors. Furthermore, CO_2 emissions are nearly unavoidable in every single step during hydrocarbon production, transportation, storage, and hydrocarbon to hydrogen conversion at the surface. Therefore, there is a substantial need to develop the new technology for clean hydrogen production while minimizing greenhouse gas footprint.

In-situ hydrogen production and extraction from petroleum reservoirs has emerged as an alternative approach to simultaneously decarbonize petroleum industry while producing clean hydrogen[4,5]. Yuan et al.[6] first proposed electromagnetic(EM)-assisted catalytic heating for in-situ hydrogen production from petroleum reservoirs[6,7]. In this approach, EM energy is delivered to the targeted formation to achieve a high enough temperature to initiate the in-situ conversion of oil and gas into hydrogen. With the assistance of downhole hydrogen membrane separators, high-concentration hydrogen gas can be extracted to the surface while all other by-products (e.g., CO, CO_2, CH_4, etc.) are simultaneously sequestrated in reservoirs, thus enabling a carbon-zero hydrogen production technology. This technology has been recently validated through lab-scale experiments in Yuan's group, with a maximum of 66 mol.% to up to 91 mol.% hydrogen being generated from oil, gas, and/or water in the presence of reservoir rocks[8–10], depending on temperatures in experiments. The techno-economic assessments showed that the hydrogen production cost by this technology can be as low as USD $0.86/kg H_2[11]and CAD $0.89/kg H_2[12], while the greenhouse gas footprint can be zero if the energy needed is completely from nearby abundant renewable energy. Despite the

* Corresponding author.
E-mail address: Qingwang.Yuan@ttu.edu (Q. Yuan).

https://doi.org/10.1016/j.applthermaleng.2024.123687
Received 23 December 2023; Received in revised form 1 May 2024; Accepted 11 June 2024
Available online 13 June 2024

significant potential of this technology, the fundamental interactions between EM waves and reservoir rocks are poorly understood, especially at high temperatures required for hydrogen production.

The utilization of EM heating for rocks and minerals has spanned several decades. In 1978, microwave heating was used for desulfurization of coal[13]. Later, relative transparency of minerals to EM energy was investigated for 40 different minerals[14]. It is found that the behavior of minerals under EM irradiation is compositionally dependent. Minerals are then classified into three categories: strong, medium, and weak absorbers, depending on their capacity to absorb EM energy and convert it into heat[15,16]. Numerous studies have explored the application of EM heating in various fields involving EM-rock interactions, including drilling[17]and grinding igneous rocks[18], processing[19]and reheating[20]minerals, accelerating curing of concrete and cement[21,22], and decarbonizing coal tar[23]. A particular focus of those studies is the rock breaking induced by EM-rock interactions. However, there is a lack of understanding on the heating behaviors especially for reservoir rocks in which different minerals may play a significant role in the heating efficiency during EM heating. A good understanding of this aspect will help better control the EM heating for maximizing the in-situ hydrogen generation from petroleum reservoirs.

One major reason for using EM heating for in-situ hydrogen production is its key feature as a rapid, selective, and direct energy transfer heating technique[24–27]. It can also penetrate rocks into a certain depth at a lower EM frequency so that a large volume of the reservoir can be heated, and hydrogen can be generated when hydrocarbons flow to the well. The fundamental mechanism for heating solid materials under EM irradiation is based on two mechanisms: ionic conduction and dielectric polarization[28,29]. Dielectric polarization mechanism is further divided into dielectric, electronic, atomic, interfacial, and orientation polarization. When EM field alternates, the dipoles within the media align with the changing electric field, leading to polarization. This alignment causes hysteresis in the molecular structure under the influence of the EM field. The resultant friction thus generates heat energy[30]. As EM waves transmit through different media, they undergo reflection, absorption, and penetration, which are primarily determined by the dielectric properties of the materials[31–33]. Dielectric constant ε' and dielectric loss factors ε'' are two key elements that characterize the dielectric response of materials under EM heating. The dielectric constant of materials reflects their ability to be polarized and store the EM energy. While the dielectric loss measures the ability to dissipate the energy as heat. Therefore, a material with a high dielectric constant absorbs more EM energy, while a material with a high dielectric loss can be easily heated by EM waves. The loss tangent, $tan\delta$, is defined as the ratio of the energy loss (ε'') to energy stored (ε') in a material, i.e., $tan\delta = \varepsilon''/\varepsilon'$, which describes the ability to convert absorbed energy into heat.

Depending on the composition of rocks and their dielectric properties, the heating behaviors are different under EM irradiation. Thermal runaway (TR) is one of the interesting phenomena in which a sudden increase in temperature is observed during the EM heating of materials such as ceramics[34], minerals[35], and cement[36]. The occurrence of TR is primarily contingent on two factors [37]: 1) the amount of heat absorbed by the material during EM irradiation; and 2) the heat loss from the heated material to the surrounding environment. TR occurs when the EM energy is absorbed and converted when generated heat is greater than a certain threshold. This threshold is a function of the heat transfer coefficient, which quantifies the amount of heat loss due to outward convection. Controlling the occurrence of TR phenomenon will avoid overheating while reducing energy consumption during in-situ hydrogen production.

In our previous studies[9,38], TR was first reported for shale and sandstone rocks in the presence of organic matter and hydrocarbons under EM heating. In fact, TR can be observed in the samples (i.e., mixture of rock, crude oil, and/or water) without iron catalysts in our first-of-the-kind work (see Exps. #3 and #7 in Figs. S6 and S7 in[8]). However, this phenomenon was not reported or investigated at that time because of the limited data. Although the research ultimately serves for the in-situ hydrogen production, the presence of hydrocarbons and artificial iron catalysts in previous studies significantly complicates the investigation of EM-induced TR of reservoir rocks because of the generation of solid carbon and reactions. The mechanism of EM heating of rock samples saturated with water is even more complex[39,40], which has a dielectric loss an order of magnitude greater than that of most minerals, thus interacting more efficiently with EM waves. Therefore, to better elucidate the underlying mechanisms of the TR phenomenon, simplified scenarios with only reservoir rocks under EM irradiation should be first examined carefully. Further, the specific roles of various minerals in different reservoir rocks during EM heating process are less unknown. The thermal behaviors of different reservoir rocks before and after the occurrence of TR are poorly understood. Given the above critical knowledge gaps, this study focuses on investigating the occurrence and underlying mechanisms of TR in both sandstone and shale rocks without hydrocarbons or artificial catalysts under EM irradiation.

In this study, two types of reservoir rocks are heated with different EM powers. To identify which minerals cause the TR phenomenon, various pure minerals are also used. Considering the potential disturbance of EM waves to communications, only the microwave frequency 2.45 GHz is used in experiments, instead of the wide EM spectrum. Advanced characterizations, such as X-ray diffraction (XRD), scanning electron microscopy (SEM), and electron probe micro-analyzer (EPMA) analysis, are conducted to characterize the mineralogical and physical changes of rocks before and after TR, aiming to understand the reasons of improved heating efficiency. This study provides a detailed explanation of the TR phenomenon and the EM-reservoir rock interactions, the insights obtained will lay a solid foundation for leveraging the TR phenomenon to achieve high heating efficiency with less energy input towards in-situ hydrogen production via the EM-assisted catalytic heating, thus shedding light on promoting the development of this emerging clean energy technology.

2. Experimental methodology

2.1. Materials

The reservoir rock samples utilized in the experiment are San Saba sandstone and Mancos shale (from Kocurek industries, Inc.). San Saba sandstone is a medium-grained sedimentary rock, mainly distributed in Texas, located in the Paleozoic formation, with a relatively loose texture and high porosity (19–21%). In contrast, Mancos shale, a fine-grained sedimentary rock, is widely distributed in the western United States. The mineralogical analysis of these two rocks, determined by XRD analysis, indicated that they contain quartz, albite, microcline, dolomite, calcite, kaolinite, illite, and chlorite, as shown in Fig. 1. All samples are crushed and sieved to a diameter range of 100–125 μm to minimize the effect of grain size on the measured results[41]. Further, pure minerals (from Rocks, Minerals and Fossils LLC) are also used for EM heating to determine their temperature profiles at different EM powers. To eliminate the effect of humidity and free water, all samples are dried in a drying oven at 70 °C at least 24 h before microwave heating.

2.2. Experimental setup

A single-mode cavity microwave system operating at a frequency of 2.45 GHz is employed to investigate the heating behaviors of reservoir rocks and pure minerals under microwave irradiation. As shown in Fig. 2, this system consists of a magnetron-type microwave generator, an E-filed cavity, a sliding short, and an auto-tuner that can automatically optimize the reflected power in real time. Before microwave heating, the sample consisting of 3 g of rock or pure mineral is loaded into the center

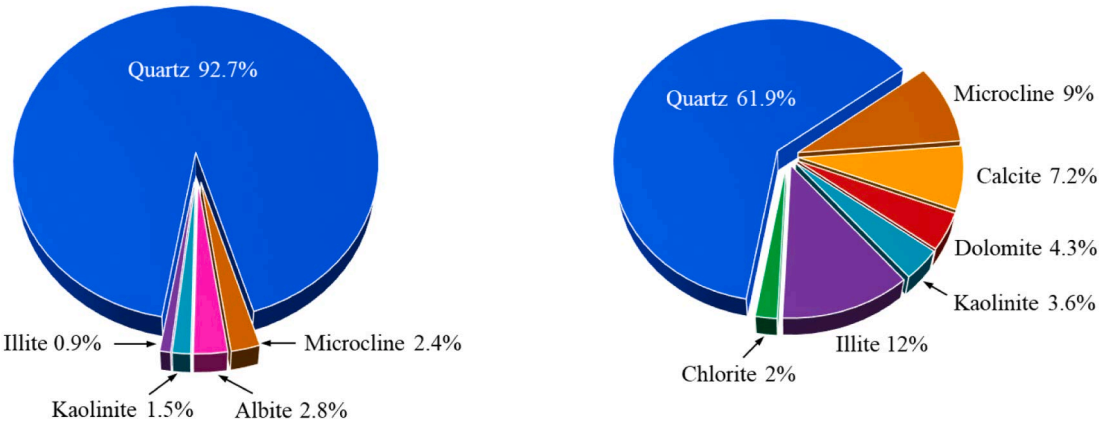

(a) San Saba sandstone (b) Mancos shale

Fig. 1. Mineral compositions of reservoir rocks.

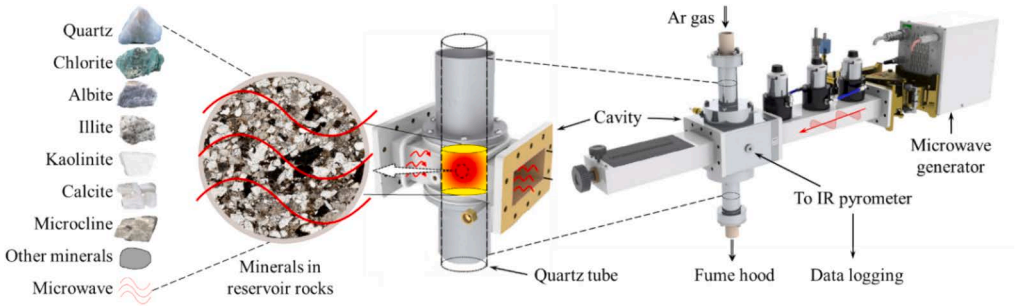

Fig. 2. Schematic for determining reservoir rock-microwave interactions.

of a quartz tube (ID 10 mm, OD 16 mm, L 36 mm), with the support of quartz wool. The loaded quartz tube is then carefully placed into the cavity. After the sealing test, argon gas (Ar) is introduced at a flow rate of 60 standard cubic centimeters per minute (sccm) into the quartz tube to maintain an inert environment throughout the heating process. Two different measurement ranges (50 °C to 400 °C and 150 °C to 1000 °C) of infrared (IR) pyrometers (2.3 μm spectral range, Micro-Epsilon) are used to monitor the real-time temperature profiles at a resolution of 0.1 °C. Because of the limitation on the minimum temperatures monitored for different IR pyrometers, 50 °C and 150 °C will be used in the temperature profiles in experiments when temperature is below them. Dielectric properties are measured between 100 MHz and 9 GHz using a Keysight P5002A vector network analyzer using coaxial transmission line method. The powdered materials of rocks and minerals are included in a paraffin wax (Sigma Aldrich) matrix at 10% volume loading, homogenized, and cast into a plug[42].

2.3. Characterization techniques

To better understand the interactions between EM-waves and rocks, advanced characterization techniques are used to analyze both fresh and spent samples. X-ray diffraction (XRD, Olympus BTX II) is utilized to quantitatively analyze the mineralogy of the samples before and after heating, with determinations performed using Co Kα radiation at a step size of 0.05 and the American Mineralogist Crystal Structure Database (AMCSD) in Xpowder software. Differential scanning calorimetry (DSC, Mettler Toledo DSC822e) is used to measure the samples' thermal properties and track the phase changes. The changes in heat flux of a 20 mg sample with increasing temperature are measured in an aluminum pan, heating from 25 °C to 600 °C at a rate of 5 °C/min at a nitrogen flow rate of 200 mL/min. Thermogravimetric Analysis (TGA, TA Instruments Q50) involved specimens in a platinum pan, under nitrogen, heating at 5 °C/min from 25 °C to 800 °C, providing detailed insight into mass changes with temperature. The elemental content of reservoir rocks is determined by X-ray fluorescence (XRF, Thermo Scientific ARL PERFORM'X) technology at 30–60 kV, 60–120 mA, and count times ranging from 8 to 40 s up on the different elements. The composition of fresh and spent samples and associated minerals is analyzed using a Cameca SX-100 with 4 WDS Spectrometers with a tungsten filament. The operation parameters are as follows: accelerating voltage at 15 kV, beam current at 20nA, and beam diameter at 0 μm for maps and minerals, except 10 μm for feldspar and 5 μm for carbonate. All X-Ray Maps are Wavelength Dispersive Spectrometer Maps (WDS, spectrometer 1 for Al and Mg, spectrometer 2 for Na, spectrometer 3 for K and Si, spectrometer 4 for Fe and Ca).

3. Results and discussions

3.1. Thermal behaviors of reservoir rocks under EM heating

3.1.1. Thermal runaway (TR) of sandstone and shale rocks

To better quantify the TR, we define the TR trigger temperature at the point when the time derivative of heating rate changes dramatically. When sandstone and shale rocks are subjected to microwave heating at an input power of 0.6 kW, their temperatures quickly increase after 4.7 min and 3.4 min, respectively, as well as the sudden changes in their heating rates as depicted in Fig. 3. The TR occurs at 568 °C for sandstone and 253 °C for shale. Apparently, the Mancos shale sample is much easier to be heated compared to the San Saba sandstone. For pure quartz sample, the temperature only reaches a maximum of 73 °C within 20 min (not shown in Fig. 3). This is due to the limited ability of quartz to absorb microwave energy, resulting in a significant portion of

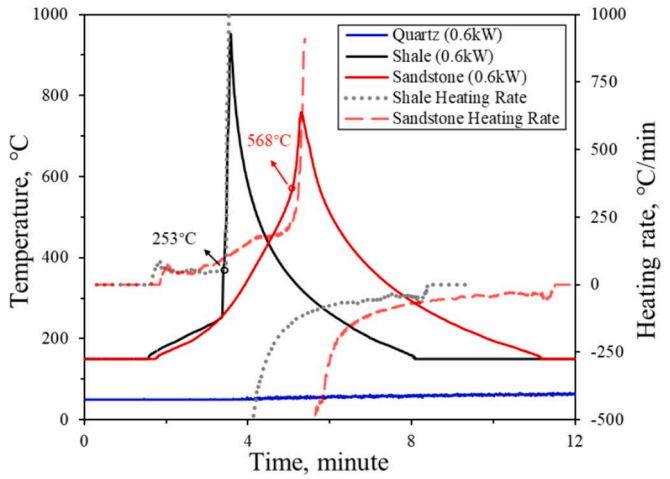

Fig. 3. Thermal behavior of rock samples.

microwave passing through the quartz sample without being converted into heat. Due to the characteristics of EM heating and the differences in mixed powder samples, the temperature profile of each microwave heating has certain differences. Additionally, adjustments made by the auto-tuner contribute to this variance. Therefore, we repeated the heating experiments to ensure that TR temperature remained within a specific range.

Before TR occurs, the temperature steadily rises at a consistent heating rate for a short period of time for both rocks. As to sandstone, the temperature begins to rise rapidly after reaching approximately 200 °C. After reaching 568 °C, the measured temperature increases much faster, exhibiting an almost vertical temperature–time relationship. For shale, the temperature abruptly soars after 253 °C, reaching an exceptionally high temperature of over 1000 °C within several seconds.

The gradual acceleration of temperature from 200 °C to 568 °C for sandstone can be attributed to the high proportion of quartz present in sandstone. As the dielectric loss of quartz increases with temperature, it enhances the overall EM energy absorption of rock samples [43]. From the atomic scale, quartz demonstrates weak and fixed electron polarization at low temperatures. However, as temperature rises, the dipoles reorient more smoothly, enhancing polarization and increasing the material's ability to couple with microwaves.

For both sandstone and shale samples, TR can occur easily at a power of 0.6 kW. However, the differences in the TR trigger temperature and trigger time indicate that different reservoir rocks have unique microwave heating behaviors and characteristics. TR occurs when the heat generated from microwave absorption surpasses the heat lost through thermal conduction.

From the perspective of heat generation by EM heating and local thermal distribution, sandstone and shale rocks are poor conductors. Therefore, the heat generated due to the local conductivity of electron charges is negligible, and dielectric loss heating dominates the heat generation process. In this scenario, higher temperatures lead to higher dielectric losses, resulting in faster heating of rock samples. Thus, it can be concluded that shale rock has higher dielectric losses compared to sandstone. This is also validated by the higher loss tangent of shale rock compared to that of sandstone in Table S1.

To further elucidate the occurrence of TR from the perspective of heat loss, Fig. 4 illustrates the changes in heating profile determined by Differential Scanning Calorimetry (DSC) and Thermogravimetric Analysis (TGA). From DSC analysis, both rocks display an overall endothermic trend when heated at a rate of 5 °C/min, suggesting an increase in their specific heat capacities and a reduced heat loss as temperature increases. The changes in enthalpy as a function of measured temperature for both rocks are crucial for explaining their reactions and phase transitions. From TGA analysis, both rocks lose mass as the temperature increases.

For sandstone, a sharp endothermic peak is observed from DSC at 573 °C in Fig. 4a. The notable peak aligns perfectly with the temperature at which the α-β phase transition of quartz occurs[44]. This phenomenon was first hypothesized based on thermal expansion experiments, suggesting that room-temperature quartz undergoes a transformation into a unique polycrystalline form upon heating at 573 °C[45]. Quartz undergoes a notable change in its dielectric properties, especially dielectric loss, during phase transitions[46]. Consequently, it can efficiently convert EM energy into heat. The quartz phase transition can also enhance the thermal properties of quartz. The specific heat capacity of quartz shows a significant increase in the vicinity of phase transition temperatures[15]. For rocks and minerals, their ability to absorb and store thermal energy depends on their specific heat[40]. Changes in specific heat capacity thus play a key role in the temperature of the rock samples. This suggests that quartz stores a substantial amount of heat during phase transition, and as the temperature rises, this stored heat is released as the specific heat capacity decreases. Therefore, it is reasonable to attribute the occurrence of TR to the changes in dielectric and thermal properties resulting from the quartz phase transition. As

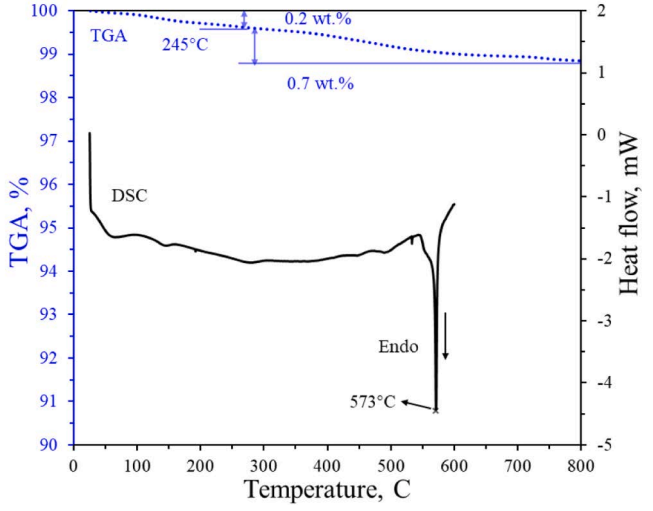

(a) Sandstone

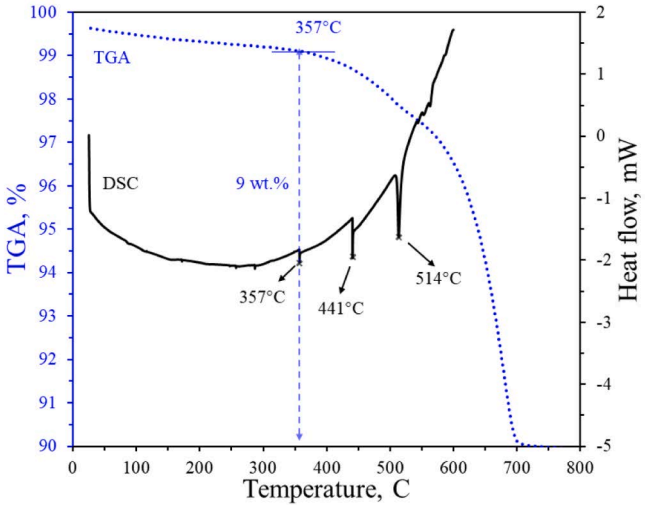

(b) Shale

Fig. 4. TGA and DSC analysis for rock samples.

temperature increases from room temperature to 245 °C, the initial 0.2 wt% mass loss primarily results from the release of absorbed, bound, and minor mineral water within the samples. From 245 °C to 800 °C, the additional 0.7 wt% weight loss is due to the decomposition of carbonates and organic materials, with minerals like illite and kaolinite decomposing between 500 °C and 600 °C[47].

In contrast, distinct peaks at 357 °C, 441 °C, and 514 °C observed in Fig. 4b for the shale sample influence the thermal properties of shale. The endothermic peaks at 357 °C and 514 °C can be attributed to the thermal decomposition of calcite and dolomite, respectively, as their decomposition temperature falls 300–420 °C[48]and around 528 °C [49]. The pyrolysis of organic matter in shale is another contributing factor to the thermal properties of shale. Depending on the properties of shale and shale oil, the pyrolysis temperature of organic matter can range from 427 °C to 464 °C[50]. Hence, the endotherm peak at 441 °C for shale rock may result from the pyrolysis of organic matter. Notably, the TGA data shows a 9 wt% weight loss in shale from 357 °C to 800 °C, which can be mainly attributed to thermal decomposition of a large amount of carbonate minerals contained in shale.

3.1.2. Disparities at various input power

When the reservoir rocks are exposed to varying input powers ranging from 0.4 kW to 1 kW, both their heating profiles and TR trigger temperatures exhibit distinct differences, as illustrated in Fig. 5. Due to different capabilities for being heated, a power of 0.6–1.0 kW is used for sandstone (Fig. 5a), while a power of 0.4–0.7 kW is used for shale (Fig. 5b). Further, when TR occurs with the sudden increase of temperature, we immediately turn the power off to avoid too high temperatures. Therefore, the values of peak temperatures in Fig. 5 are not essential.

Overall, both rocks exhibit a reduced TR trigger temperature and an accelerated occurrence time of TR as the input power increases. This is because of the competition between heating by microwave energy absorption and conduction at different power levels. More specifically, these observations can be attributed to the following reasons. First, the dielectric properties are temperature dependent. Dielectric constant and dielectric loss both increase with temperature, especially during phase transition. A significant increase in dielectric loss could shift the rocks from weak to strong microwave absorption[51]. Second, quartz is characterized as a microwave transparent material at lower temperatures. Microwaves efficiently pass through quartz and directly heat the microwave absorption minerals. Different local conductivities present in different minerals can cause thermal heterogeneity. This leads to the generation of hotspots where a substantial amount of heat accumulates locally. A higher input power exacerbates the imbalance between EM absorption and heat loss, thereby triggering faster thermal runaway. Third, thermal conductivity remains constant at a given temperature. However, variations in accumulated heat result in differences in the required temperature and time for heat to transfer from the center of the sample to the surface under varying power levels.

When comparing sandstone and shale rocks, distinct heating patterns are observed. Sandstone consistently exhibits accelerated heating until it reaches TR at various power levels, demonstrating that power differences significantly influence the entire heating process. In contrast, shale displays a relatively consistent heating profile with a clear TR trigger temperature, enabling easy delineation of the temperature profile into two regions: before and after TR. Before TR, the temperature in shale is affected by the power level, while after TR, shale rapidly reaches temperatures exceeding 800 °C within seconds even at a microwave power as low as 0.4 kW.

3.2. The role of mineralogy and chemical elements

Rocks, as a mixture formed through geological processes involving various minerals, exhibit responses to EM heating that are closely related to the combination and interaction of their mineral components. The interactions influencing rock heating encompass the intrinsic properties of minerals, mineralogical and chemical composition of rocks, proportions of various minerals, and decomposition of minerals, etc.

Analyses of the primary mineral components and elements of two rocks are conducted due to their significant influence on thermal behavior under EM heating. Given the relatively minor proportion of cementing substances and trace elements in rocks, their impact during the microwave heating process is considered negligible [52]. Table 1 shows the eight identified minerals and chemical formulas identified in both rocks. Fig. 6a summarizes the heating profiles for these pure

Table 1
Chemical formula for the mineral content in rock samples.

Mineral	Chemical formula
Quartz	SiO_2
Albite	$Na(AlSi_3O_8)$
Chlorite	$(Mg, Fe^{2+})_5Al_2Si_3O_{10}(OH)_8$
Illite	$K_{0.6}(H_3O)_{0.4}Al_{1.3}Mg_{0.3}Fe^{2+}_{0.1}Si_{3.35}O_{10}(OH)_2{\cdot}(H_2O)$
Kaolinite	$Al_2Si_2O_5{\cdot}(OH)_4$
Microcline	$K(AlSi_3O_8)$
Calcite	$CaCO_3$
Dolomite	$CaMg(CO_3)_2$

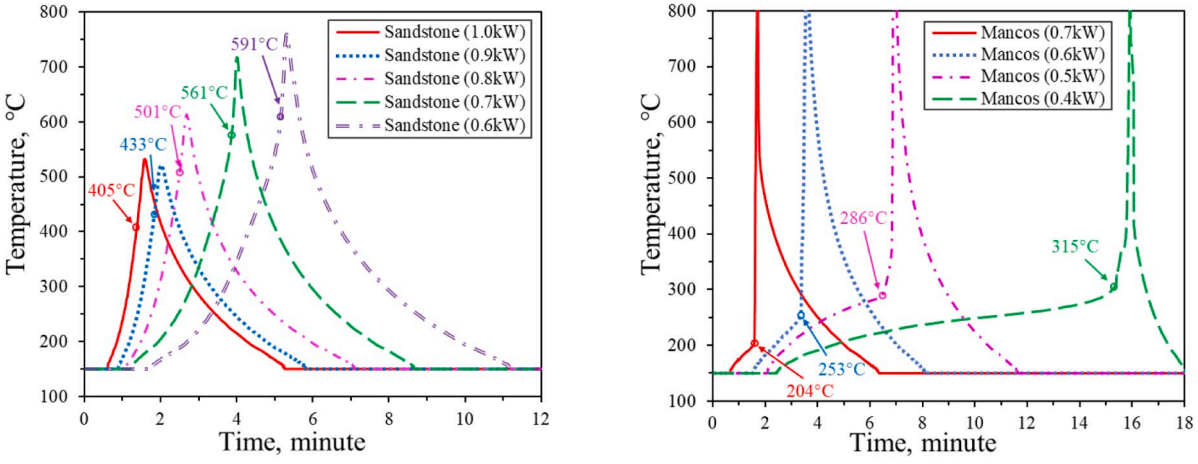

(a) San Saba sandstone (b) Mancos shale

Fig. 5. Temperature profiles of reservoir rocks at various input power.

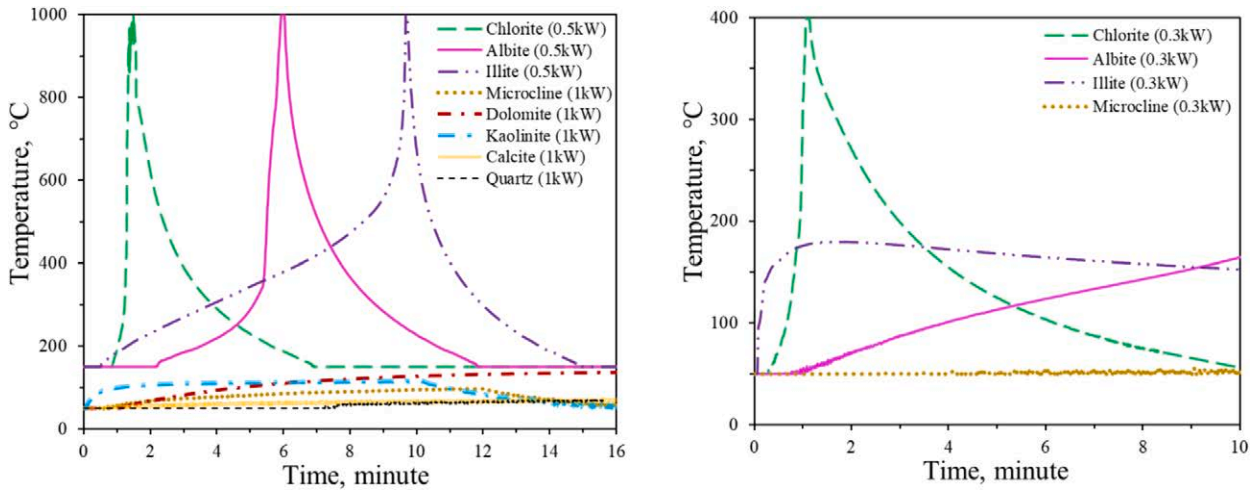

Fig. 6. Temperature profile of pure minerals at various input powers.

minerals. It can be seen that TR occurs easily for chlorite, albite, and illite at a lower input power of 0.5 kW, whereas the maximum temperatures of microcline, dolomite, kaolinite, calcite, and quartz are less than 150 °C after heating for 10 min at a power of 1 kW without TR being observed.

Fig. 6 indicates that chlorite, albite, and illite are strong microwave absorption minerals and play a key role in the occurrence of TR of reservoir rocks. Illite initially exhibits a strong microwave response, characterized by a rapid temperature increase below 200 °C, followed by a later occurrence of TR (Fig. 6a) and a decrease after peaking (Fig. 6b). This is attributed to the endothermic dehydration reaction, leading to a slower temperature increase or even a decrease at a lower microwave power[53]. The capability of Illite to swiftly convert EM energy into heat makes it a significant contributor to the initial temperature rise during the EM heating of reservoir rocks.

In contrast, chlorite has the strongest ability to be heated under microwave irradiation. This may result from the presence of metallic elements such as magnesium (Mg) and ferrum (Fe) which are considered to better interact with microwaves (Lu et al., 2017). Albite, despite having a composition close to microcline, exhibits different heating profiles. This variation could be attributed to a more effective response to microwave energy of sodium (Na) compared to potassium (K), or to the differing crystal structures of albite and microcline[54,55]. Structural differences between albite, which consists of an interconnected framework of three SiO_4 and one AlO_4 tetrahedron, and fully ordered triclinic microcline feldspar led to different dipole moment and polarization ability. For minerals with weak microwave absorption capability, microcline, dolomite, kaolinite, and calcite do not show an obvious contribution to enhance the microwave heating. Calcite and dolomite display a high dielectric constant and low dielectric loss[51], suggesting that calcite absorbs and stores a significant amount of EM energy but does not convert it into thermal energy.

The heating behavior of three minerals with good microwave absorption capability is depicted in Fig. 6b at a lower power of 0.3 kW. For comparison, the heating profile of microcline is also plotted. Particularly, TR occurs for chlorite even at such low power in around one minute. Illite and albite can also be easily heated to nearly 200 °C within 10 min. In contrast, microcline can be heated to 53 °C after 10 min of EM exposure, while the other four minerals cannot reach the minimum measurement range of the IR pyrometer (50 °C), which are not included in Fig. 6b. These five pure minerals have weak microwave absorption properties and are unable to enhance heating efficiency, even under higher microwave power conditions.

Considering the excellent ability for absorbing microwave, even a small amount of chlorite, albite, and illite in reservoir rocks can significantly enhance EM heating. They may act as a natural promoter to heat the surrounding minerals and contribute to a higher overall heating efficiency of reservoir rocks. Furthermore, the non-uniform distribution of these three minerals in reservoir rocks will most likely cause the hot spots to be distributed locally and non-uniformly in the samples during EM heating. This is an intrinsic feature of EM heating, even for the simpler cases with only catalysts and hydrocarbons at the surface applications[56,57]. Such temperature inhomogeneity may be more severe because of the TR phenomenon occurring in reservoir rocks.

The variations in heating behaviors mentioned above are attributed to the distinct mineral compositions of the two rock types. The sandstone consists of 92.7% quartz, 2.4% microcline, 0.9% illite, and 2.8% albite as shown in Fig. 1, with the latter two minerals acting as strong microwave absorption minerals and aiding in the heating of sandstone under microwave radiation. As previously emphasized, pure quartz is difficult to heat up to the TR trigger temperature. This underscores the importance of other minerals in sandstone in enhancing microwave heating and the occurrence of TR. Illite, with its ability to efficiently convert microwave energy to heat, contributes to the formation of hotspots within the sandstone initially, thus heating the surrounding minerals. Albite, in contrast, responds well to microwave at higher temperatures for heating the rocks.

Mancos shale sample has a more complex mineral composition compared to sandstone. Minerals such as microcline, calcite, dolomite, and kaolinite are weak microwave absorption minerals, collectively accounting for 24.1 wt% of shale. Comprising 14 wt% of the total mineral content in shale, illite, and chlorite play a crucial role in triggering TR at a lower power compared to sandstone (see Fig. 5). Further explanation can be found in the quantitative chemical element data obtained using XRF as shown in Fig. 7, which indicates the metal elements in shale are apparently higher than sandstone. These metal elements, especially ferrum, can enhance the loss tangent, thereby increasing EM waves absorbed capacity via the improvement of polarization effects.

3.3. *Heating behavior after thermal runaway*

During in-situ hydrogen production from petroleum reservoirs, the EM heating may be paused and restarted because of the operations and the usage of intermittent renewable energy. In this section, the heating behaviors of post-TR rocks are investigated without involving hydrocarbons in the rock samples. This simplification can avoid the complexity and interferences because of the hydrocarbons and solid carbon in our previous studies[9,38], thus allowing a better understanding of interactions between EM waves and rocks.

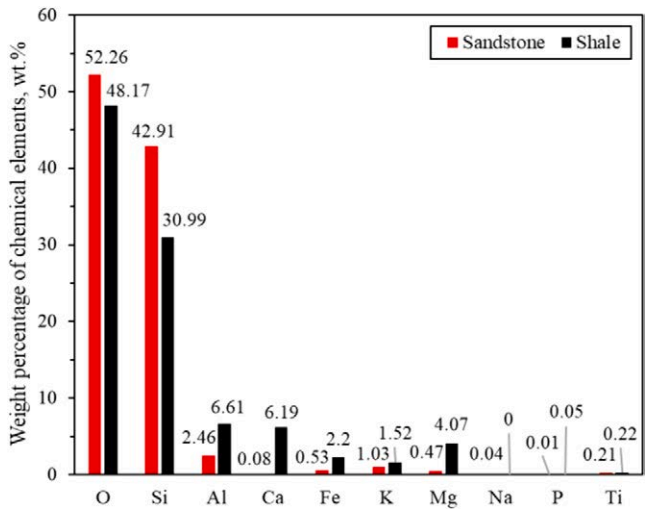

Fig. 7. Chemical elements proportion of San Saba sandstone and Mancos shale rocks.

3.3.1. *Improved heating efficiency*

For sandstone rocks, Fig. 8a shows that the post-TR sandstone rocks can be easily heated to higher temperatures at lower microwave powers compared to the fresh sandstones before TR (Fig. 5a). At 0.2 kW, even TR does not occur for the post-TR sandstone sample due to the low power. The temperature of the post-TR sandstone (purple curve in Fig. 8a) is even higher than that of fresh sandstone at a higher power of 0.5 kW (red solid curve). As power increases from 0.2 kW to 0.5 kW, TR occurs earlier and temperature rises more rapidly, aligning with the trend described in section 3.1.2. Specifically, fresh sandstone sample can only be heated up to 213 °C after 20 min at 0.5 kW (solid red curve), while the post-TR sample can reach 800 °C within 1 min at the same input power. In other words, TR happens again and easier (dashed red curve). These observations clearly demonstrate the enhanced heating efficiency because of the occurrence of previous TR phenomenon.

Notably, the TR trigger temperatures of the post-TR sandstone sample at various input powers (for example, 537 °C at 0.4 kW and 578 °C at 0.3 kW) are close to the phase transition temperature of quartz, which is 573 °C (Fig. 4a). This indicates a strong correlation between the occurrence of TR and the thermal behavior of quartz. The α-β phase transition in quartz is displacive, involving only the rearrangement of atoms in the Si-O network without breaking chemical bonds. Consequently, this phase transition is reversible, with quartz existing in the β phase above the transition temperature and reverting to the α phase as the temperature drops. Hence, once temperature of the rock samples reduces to room temperature after microwave heating is stopped, this reversible transformation is manifested by the recurrence of TR for post-TR sandstone, elucidating the mechanisms for TR for post-TR sandstone samples.

Note in Fig. 8a, one test is conducted at each microwave power. Considering the temperature inhomogeneity discussed in section 3.2, there is an uncertainty on the measured temperatures during EM heating. There is no need to repeat all experiments for all rock samples. Here, we only repeat it five times for both fresh and post-TR shale rock samples by EM heating at 0.18 kW, as shown in Fig. 8b. The step-heating experiments were also performed for comparison and for the analysis of energy efficiency later. Since all shale rock powders were made together and mixed uniformly as much as we can, the samples have nearly the same particle size and composition but with unavoidable, slight differences. Because of these reasons, it is expected that there is a small temperature range for the five repeated experiments. Additionally, the temperatures may vary if different microwave generators (magnetron and solid state), designs, and manufacturers are used by different research groups. Thus, repeating the experiments five times will provide a pretty good quantification of the uncertainties on temperatures.

As shown in Fig. 8b, the post-TR shale sample exhibits a more controllable temperature profile at a low microwave power. At 0.18 kW, the fresh shale can achieve a maximum temperature of 139–192 °C (light blue band), whereas the post-TR shale sample can be heated to 806–878 °C at a constant power of 0.18 kW (red band), illustrating a significant improvement of heating efficiency after TR. The step heating scenarios were also examined, with a much higher temperature achieved for the post-TR shale sample at 0.10 kW than that of 0.18 kW for fresh sample. The temperatures of the post-TR shale samples continuously rise as the microwave power increases from 0.10 kW to 0.18 kW step by step. Eventually, a similar maximum temperature range (pink band) is achieved with the scenario at a constant power of 0.18 kW. It is expected that the temperatures for post-TR shale at a higher microwave power (e.g., >0.5 kW) may immediately reach above 1000 °C in the first several minutes (not shown in Fig. 8b). The quantification on heating behaviors for post-TR reservoir rocks can benefit temperature control and energy efficiency in the in-situ hydrogen production technology.

To further quantify the improvement in heating efficiency for post-TR rock samples, the power saved and energy consumed are calculated, as depicted in Fig. 9. Power saved is calculated based on the powers required by the fresh and the post-TR samples to achieve the

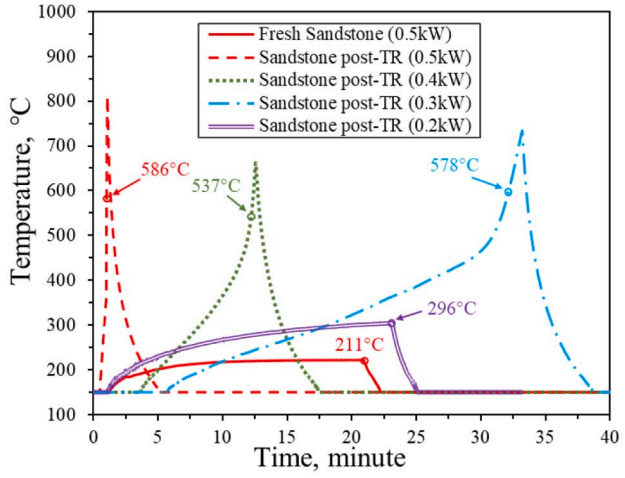

(a) San Saba sandstone

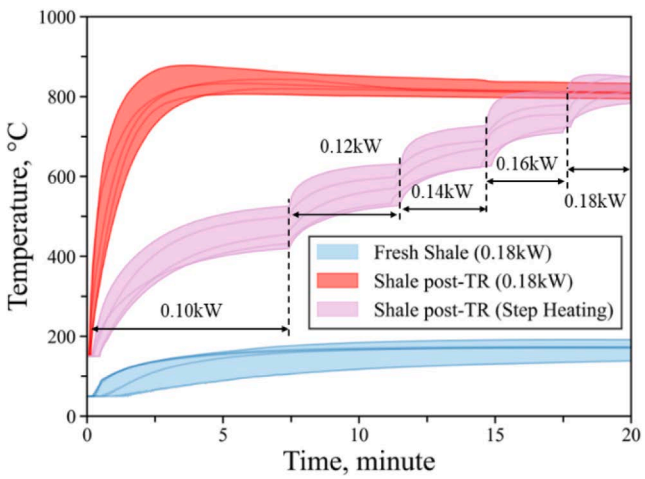

(b) Mancos shale (five curves for each scenario).

Fig. 8. Temperature profile of post-TR reservoir rocks under various input powers.

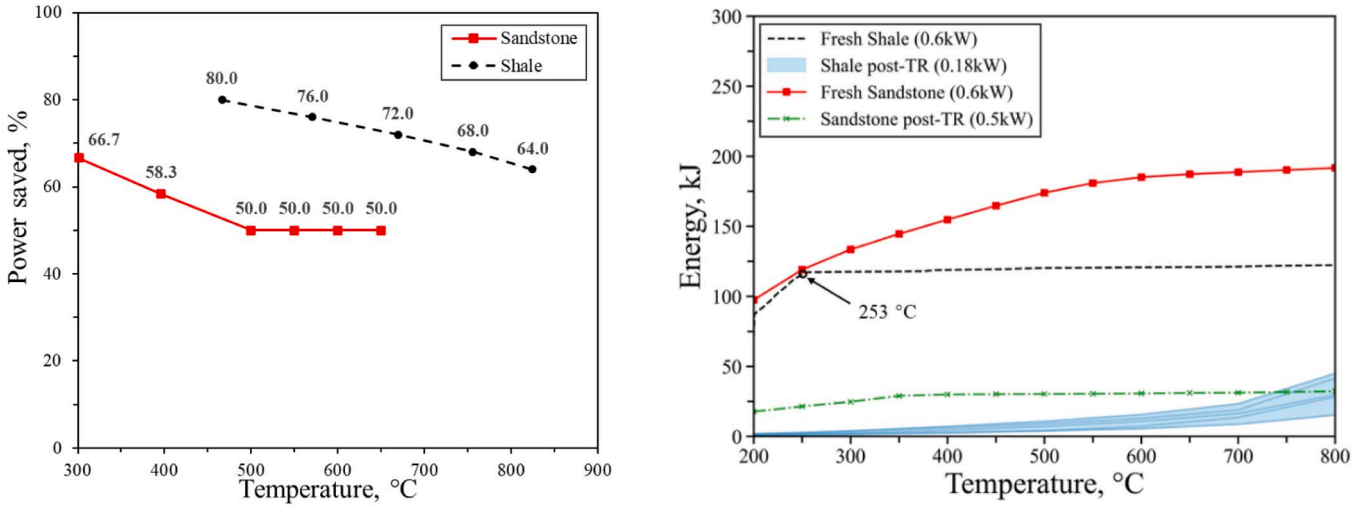

(a) Power saved (b) Energy consumed

Fig. 9. Comparison of power and energy for post-TR samples at various temperatures (In Fig. 9b, the shale post-TR sample initially reaches TR at 0.6 kW and is then heated at 0.18 kW; the sandstone post-TR sample first reaches TR at 0.6 kW and is then heated at 0.5 kW).

same temperatures. Energy consumption is defined as the total input energy needed for different rock samples to reach the specific temperatures during the heating process, which is determined by both the used microwave power and the required heating time. Our objective is to analyze the reduction of energy consumption caused by TR occurrence; therefore, energy consumed before TR is not included in the calculations.

For post-TR sandstone samples, the maximum power saved reaches 66.7% compared with fresh sandstone to achieve 300 °C,as shown in Fig. 9a. To achieve 500–650 °C, the powers saved are 50%. In comparison, the powers saved for post-TR shale rocks are obviously higher than post-TR sandstone samples, ranging from 80.0% to 64.0% as temperature increases from 450-850 °C. This finding indicates that the TR occurrence can be leveraged to significantly improve the heating efficiency of reservoir rocks, therefore reducing the input energy during the heating process and lowering the cost of in-situ hydrogen generation.

Fig. 9b shows the comparison of energy consumed to achieve certain temperatures for both fresh and post-TR reservoir samples. Clearly, post-TR shale samples (light blue band) need substantially less energy to achieve the same temperatures compared to the fresh shale sample (dashed black curve). This is caused not only by the reduction of input power to heat the post-TR shale rock, but also by the shorter time required compared to the fresh sample. Once TR occurs at the temperature of 253 °C, the temperature rises rapidly. Consequently, the energy consumption after TR increases slightly for shale samples. For post-TR sandstone sample as shown in the green curve, it is evident the energy consumption is also significantly reduced compared to the fresh sample (red curve).

3.3.2. *Characterizations*

To understand the mineralogical changes of the rock samples after EM heating, the XRD analyses were conducted for both sandstone and shale rocks, as shown in Fig. 10a. Fresh sandstone exhibits strong quartz characteristic peaks, with a small peak for albite observable at 2θ ≈32.5°. For the post-TR samples, quartz peaks remain visible but are

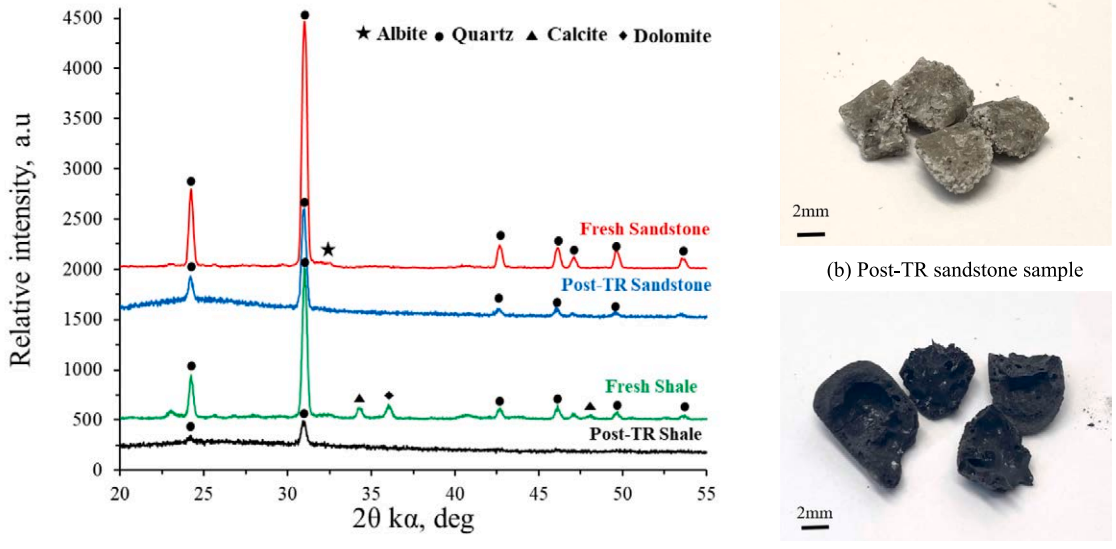

(a) XRD results of fresh and post-TR rock samples (b) Post-TR sandstone sample (c) Post-TR shale sample

Fig. 10. Characterizations of rock samples.

apparently reduced in intensity, reflecting alterations of the crystal structure in quartz. Different structural forms of quartz have varying dielectric properties, so the high temperatures during thermal runaway can alter the quartz structure, thus increasing the total dipole moment and enhancing the material's EM heating capacity. Moreover, the increase of tanδ for the post-TR samples, as listed in Table S1, confirms the improved dielectric properties of quartz after TR.

When it comes to the fresh and post-TR shale samples, the XRD analysis distinctly shows the loss of characteristic calcite and dolomite peaks, in line with the thermal decomposition of these minerals discussed in section 3.1. Notably, post-TR shale exhibits only a weak quartz diffraction peak at $2\theta = 31^{\circ}$, suggesting reduced crystallinity after thermal runaway. This implies that the high temperatures and reactions among minerals cause the post-TR shale to become a fused, glass-like mixture, thereby diminishing some of its crystalline features and subsequently altering its thermal properties. The post-TR shale curve reveals the disappearance of characteristic calcite and dolomite peaks, aligning with the thermal decomposition of these minerals discussed in Section 3.1. Employing Energy-Dispersive Spectroscopy (EDS), fresh and post-TR sandstone and shale samples are analyzed in Fig. S1. The variation in elemental composition between fresh and spent samples provides indirect evidence supporting this observation. An observed increase in Si content in the spent shale indicates the thermal decomposition of other minerals, leading to a relative increase in quartz content.

The photographs of the centrally clumped regions of the samples after microwave heating are shown in Fig. 10b and 10c. The samples transition from loose powders to glass-like clumps, indicating mineral partial melting due to high internal temperatures. This transformation also corroborates the peak changes observed in the XRD analysis of quartz samples. Additionally, the formation of cavities and fractures within the post-TR shale samples, as illustrated in Fig. 9c, is likely due to gas release during the thermal decomposition of calcite and dolomite in the TR process.

To further understand the mineral and compositional changes, electron probe analysis and Wavelength-Dispersive X-Ray spectroscopy (WDS) mapping are performed for samples before and after EM heating, as illustrated in Fig. 11. The mineral phases indicate that fresh sandstone primarily consists of quartz, with some microcline and albite, similar to the mineral composition depicted in Fig. 2a. However, for the post-TR sandstone, it seems the quartz grains are well surrounded by microcline minerals, while the albite is less observed as shown in Fig. 11b. This may result from the mineral fusion caused by the high temperature during TR. For fresh shale, distributions of microcline, albite, kaolinite, illite, chlorite, and dolomite are observed. In post-TR shale, a clear reduction in dolomite is noted, with some cavities also observed on the surface of the minerals. This further confirms the thermal decomposition of dolomite.

It is noteworthy that the shapes of particles in rock samples also undergo significant changes during the TR process. In fresh samples, the mineral particles are round and oval with smooth edges. While in post-TR samples, the edges of the particles become sharp and irregular, accompanied by debris. These changes can be attributed to two main factors. First, high temperatures cause the minerals to melt in post-TR samples, leading to the formation of clumps. Subsequently, mechanical grinding contributes to the disintegration of particles, resulting in

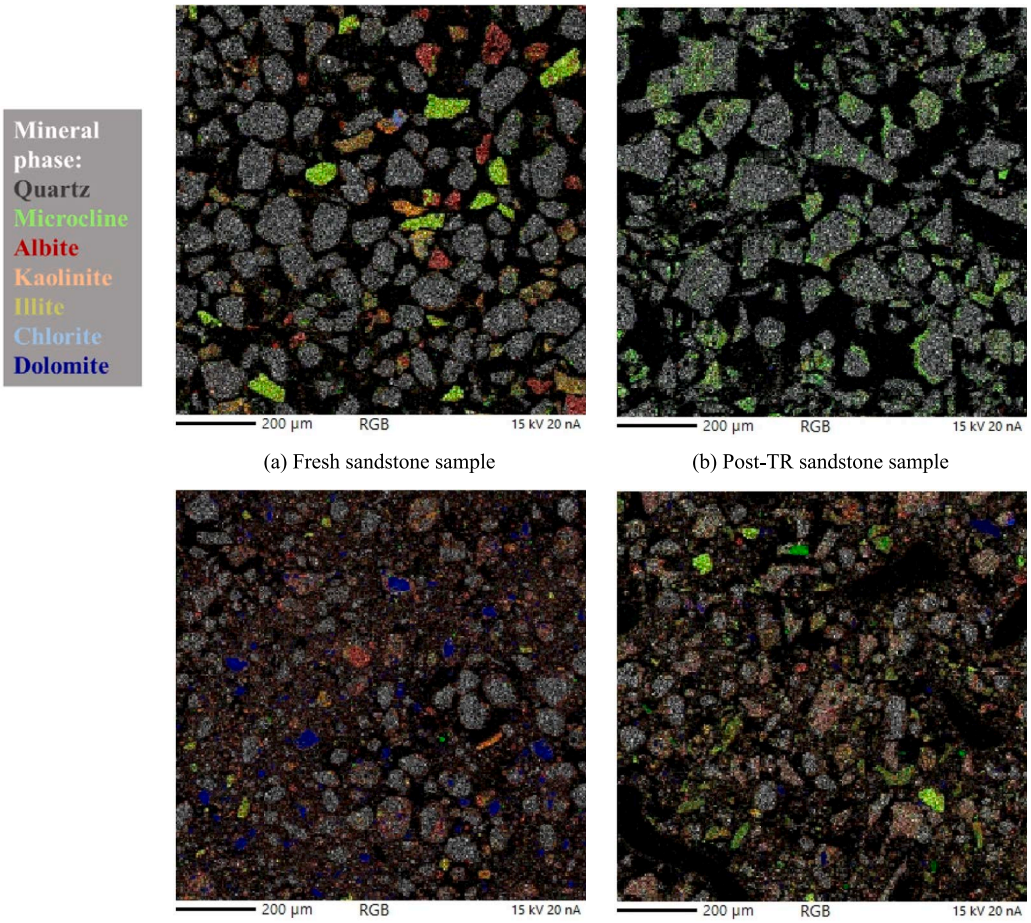

(a) Fresh sandstone sample (b) Post-TR sandstone sample

(c) Fresh shale sample (d) Post-TR shale sample

Fig. 11. WDS map for fresh and spent rock samples.

irregular boundaries. Moreover, the varying absorption capacities of different minerals for EM waves result in distinct thermal expansions. This differential expansion creates stress among the minerals, leading to their fragmentation and shattering.

The topographical changes of sandstone and shale rocks before and after microwave heating are also examined, as depicted by the SEM images in Fig. 12. Fresh sandstone samples mainly comprise regular quartz crystals and various mineral grains. After TR, the rocks with the cleavage planes—smooth surfaces along which a mineral crystal splits under an applied force in a specific crystalline direction—are more pronounced, exhibiting clearer and more distinct quartz cleavage steps, as shown in Fig. 12b. Comparing Fig. 12c and 12d, the shale exhibits a similar trend, transitioning from a disordered arrangement of mineral grains and clasts to a more structured organization. Noticeably, numerous strip-like cracks are evident on the surface of the spent rocks. These can be attributed to the thermal expansion of internal mineral components during microwave rock heating, which leads to the development of intergranular and *trans*-granular cracks as well as dimples. Furthermore, when TR occurs, the extreme thermal gradient contributes to thermal stress that encourages crack propagation. This will especially benefit the fluid flows in shale reservoirs and tight sandstone reservoirs for in-situ hydrogen generation and extraction.

4. Conclusions

This study provides new insights into the intricate interactions between EM heating and reservoir rocks, particularly highlighting the role of minerals in reservoir rocks towards in-situ hydrogen production from petroleum reservoirs using EM-assisted catalytic heating. Several important conclusions can be drawn.

During EM heating, shale exhibits a more pronounced heating behavior compared to sandstone rock. The TR trigger temperature of Mancos shale is 253 °C, lower than 568 °C for San Saba sandstone rock. TR occurs earlier at a higher EM power while the TR trigger temperature decreases, which is determined by the competition between heat accumulation and heat conduction from the rock samples during EM heating.

Different minerals in reservoir rocks behave differently under EM irradiation. Strong EM-absorbing minerals, such as chlorite, albite, and illite, play a crucial role in enhancing EM heating and initiating the TR phenomenon. Mancos shale rock can be heated easier with TR occurring earlier due to its higher content of these minerals compared to San Saba sandstone. The distinction between strong and weak EM absorption minerals also lies in their metallic elements, like Fe and Mg. These elements aid the minerals in coupling with EM waves, thereby enhancing their heating efficiency. Further, the α-β phase transition of quartz at

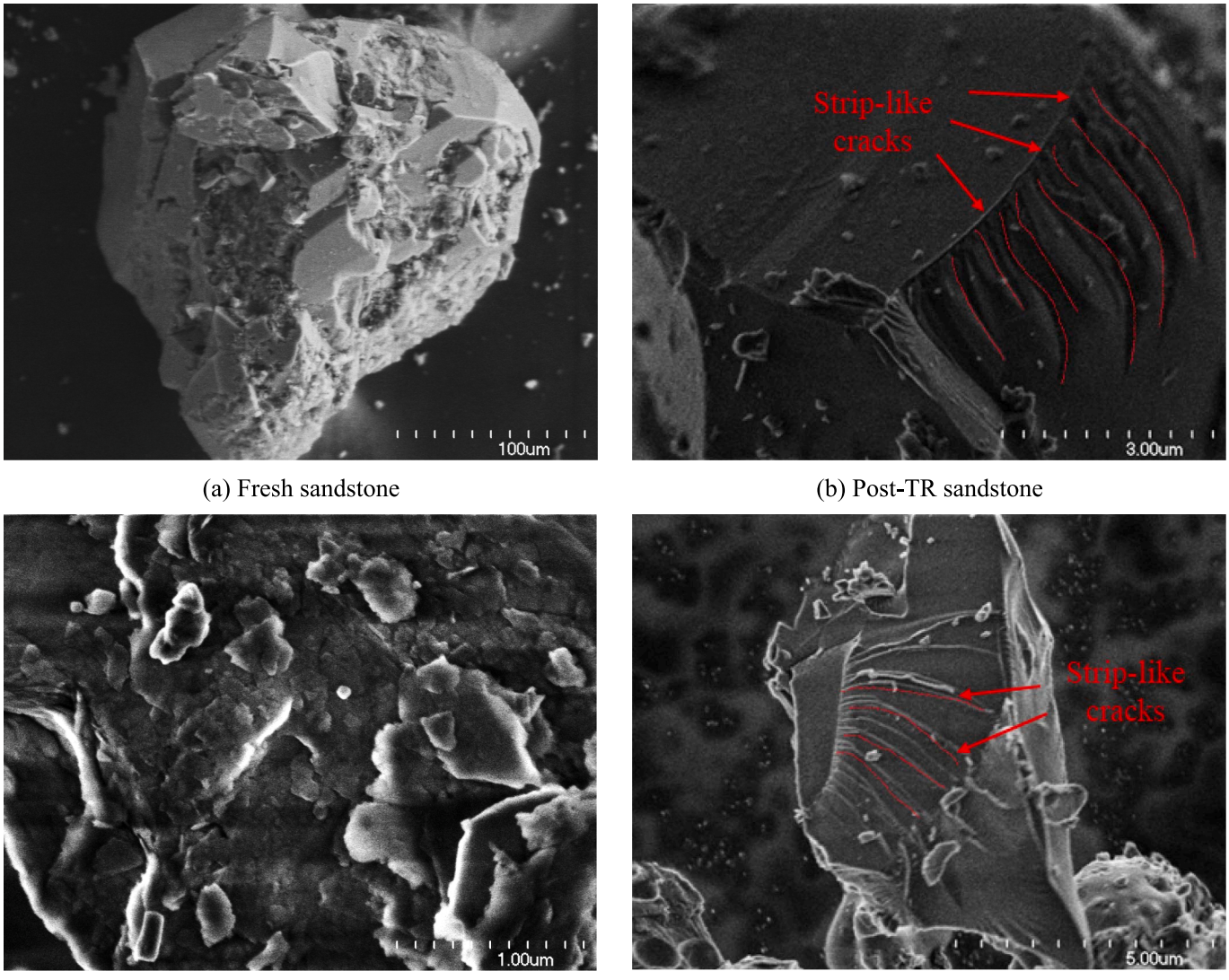

(a) Fresh sandstone (b) Post-TR sandstone

(c) Fresh shale (d) Post-TR shale

Fig. 12. SEM analysis of San Saba sandstone and Mancos shale rocks.

high temperatures significantly changes the dielectric and thermal properties of reservoir rocks, contributing to the occurrence of TR.

Once TR occurs, the post-TR reservoir rock samples, both sandstone and shale, can be reheated to high temperatures. TR occurs again to the post-TR sandstone rocks, which can be attributed to the reversibility of the quartz phase transition. In comparison, very high temperatures can be easily achieved for post-TR shale samples at low EM powers. Non-uniform heating is observed during EM heating with the temperature ranges being well quantified in this work. Overall, powers saved for heating the post-TR sandstone and shale samples vary from 50.0-66.7% and 64.0–80.0%, respectively, compared to heating the fresh rock samples. The powers need to be optimized to minimize the energy consumption for heating the post-TR rocks by integrating the insights obtained in this lab-scale research.

This work lays a solid foundation for controlling the temperatures, avoiding overheating, and increasing energy efficiency using EM heating for in-situ hydrogen production from petroleum reservoirs. It de-risks the emerging in-situ clean hydrogen technology via EM-assisted heating.

CRediT authorship contribution statement

Baizheng An: Writing – review & editing, Writing – original draft, Methodology, Data curation, Formal analysis, Investigation, Validation, Visualization. **Keju Yan:** Writing – review & editing, Validation, Formal analysis, Investigation, Visualization. **Brandon Robinson:** Investigation. **Jianli Hu:** Investigation. **Qingwang Yuan:** Writing – review & editing, Validation, Supervision, Resources, Conceptualization, Investigation, Methodology, Formal analysis, Funding acquisition, Visualization.

Declaration of competing interest

The authors declare that they have no known competing financial interests or personal relationships that could have appeared to influence the work reported in this paper.

Data availability

Data will be made available on request.

Acknowledgement

This work is supported by the donors of ACS Petroleum Research Fund under Doctoral New Investigator Grant 66828-DNI5 and the National Science Foundation under Award No. 2247676. Q.Y. thanks the Matejek Family Faculty Fellowship. The authors also thank Mr. Cecil Millikan for technical support on the microwave reactor system.

Appendix A. Supplementary data

Supplementary data to this article can be found online at https://doi.org/10.1016/j.applthermaleng.2024.123687.

References

[1] B. Fattouh, R. Poudineh, R. West, The rise of renewables and energy transition: what adaptation strategy exists for oil companies and oil-exporting countries? Energy Transitions 3 (1) (2019) 45–58, https://doi.org/10.1007/S41825-019-00013-X.
[2] S. Nižetić, M. Arıcı, A.T. Hoang, Smart and Sustainable Technologies in energy transition, J. Clean. Prod. 389 (2023) 135944, https://doi.org/10.1016/J.JCLEPRO.2023.135944.
[3] P. Sun, B. Young, A. Elgowainy, Z. Lu, M. Wang, B. Morelli, T. Hawkins, Criteria air pollutants and greenhouse gas emissions from hydrogen production in U.S. steam methane reforming facilities, Environ. Sci. Tech. 53, 12 (2019) 7103–7113, https://doi.org/10.1021/ACS.EST.8B06197.
[4] P.R. Kapadia, M.S. Kallos, I.D. Gates, Potential for hydrogen generation from in situ combustion of Athabasca bitumen, Fuel 90 (2011) 2254–2265, https://doi.org/10.1016/J.FUEL.2011.02.038.
[5] P.R. Kapadia, J. Wang, M.S. Kallos, I.D. Gates, Practical process design for in situ gasification of bitumen, Appl. Energy 107 (2013) 281–296, https://doi.org/10.1016/j.apenergy.2013.02.035.
[6] Q. Yuan, X. Jie, B. Ren. High-purity, CO_2-free hydrogen generation from crude oils in crushed rocks using microwave heating. Proceedings - SPE Annual Technical Conference and Exhibition 2021-September, 21–23 (2021). https://doi.org/10.2118/206341-MS.
[7] Q. Yuan, B. Ren, In-situ hydrogen generation and production from petroleum reservoirs, The World Intellectual Property Organization, March 2023. Patent PCT/US2022/044109,.
[8] Q. Yuan, X. Jie, B. Ren, Hydrogen generation in crushed rocks saturated by crude oil and water using microwave heating, Int. J. Hydrogen Energy 47 (2022) 20793–20802, https://doi.org/10.1016/J.IJHYDENE.2022.04.217.
[9] K. Yan, B. An, Q. Yuan, Unraveling the role of water in microwave/electromagnetic-assisted catalytic heating for hydrogen production from gas reservoirs. Proceedings - SPE Annual Technical Conference and Exhibition 2023-October, 16–18 (2023a). https://doi.org/10.2118/214884-MS.
[10] K. Yan, X. Jie, X. Li, J. Horita, J. Stephens, J. Hu, Q. Yuan, Microwave-enhanced methane cracking for clean hydrogen production in shale rocks, Int. J. Hydrogen Energy 48 (41) (2023) 15421–15432, https://doi.org/10.1016/J.IJHYDENE.2023.01.052.
[11] P. Sun, V. Cappello, K.H. Baek, Technoeconomic analysis (TEA) and life cycle analysis (LCA) on the in-situ hydrogen production with electro-magnetic heating. Energy Systems and Infrastructure Analysis (ESIA) Division Argonne National Laboratory (2023). https://www.terra-vent.com/learn.
[12] C.D. Neufeld, Techno economic feasibility of a hydrogen supply using in-situ generation from hydrocarbons with catalysts and electromagnetic heating, University of Calgary, 2023. MSc thesis.
[13] P.D. Zavitsanos, Coal desulfurization using microwave energy. environmental protection agency, office of research and development, office of energy, minerals, and industry, industrial, Environ. Res. (1978).
[14] T.T. Chen, J.E. Dutrizac, K.E. Haque, W. Wyslouzil, S. Kashyap, The relative transparency of minerals to microwave radiation, Can. Metall. q. 23 (3) (1984) 349–351, https://doi.org/10.1179/CMQ.1984.23.3.349.
[15] P. Hartlieb, M. Toifl, F. Kuchar, R. Meisels, T. Antretter, Thermo-physical properties of selected hard rocks and their relation to microwave-assisted comminution, Miner. Eng. 91 (2016) 34–41, https://doi.org/10.1016/J.MINENG.2015.11.008.
[16] M. Toifl, R. Meisels, P. Hartlieb, F. Kuchar, T. Antretter, 3D numerical study on microwave induced stresses in inhomogeneous hard rocks, Mineral Engineering 90 (2016) 29–42, https://doi.org/10.1016/J.MINENG.2016.01.001.
[17] F. Hassani P. Radziszewski J. Ouellet M. Nokkent P. Nekoovaght Microwave Assisted Drilling and Its Influence on Rock Breakage a Review 2008 ISRM pp. ISRM-ARMS5.
[18] S.W. Kingman, W. Vorster, N.A. Rowson, The influence of mineralogy on microwave assisted grinding, Miner. Eng. 13 (3) (2000) 313–327, https://doi.org/10.1016/S0892-6875(00)00010-8.
[19] S.W. Kingman, Recent developments in microwave processing of minerals, Int. Mater. Rev. 51 (2006) 1–12, https://doi.org/10.1179/174328006X79472.
[20] E. Lester, S. Kingman, The effect of microwave pre-heating on five different coals, Fuel 83 (2004) 1941–1947, https://doi.org/10.1016/J.FUEL.2004.05.006.
[21] P. Rattanadecho, N. Makul, A. Pichaicherd, P. Chanamai, B. Rungroungdouyboon, A novel rapid microwave-thermal process for accelerated curing of concrete: Prototype design, optimal process and experimental investigations, Constr. Build. Mater. 123 (2016) 768–784, https://doi.org/10.1016/J.CONBUILDMAT.2016.07.084.
[22] W. Wei, Z. Shao, R. Qiao, W. Chen, H. Zhou, Y. Yuan, Recent development of microwave applications for concrete treatment, Constr. Build. Mater. 269 (2021) 121224, https://doi.org/10.1016/J.CONBUILDMAT.2020.121224.
[23] Y. Yan, S. Gonzalez-Cortes, B. Yao, X. Jie, H. AlMegren, F. Cao, J. Dilworth, D. R. Slocombe, T. Xiao, P.P. Edwards, The decarbonization of coal tar via microwave-initiated catalytic deep dehydrogenation, Fuel 268 (2020) 117332, https://doi.org/10.1016/J.FUEL.2020.117332.
[24] Q. Li, X. Li, T. Yin, Effect of microwave heating on fracture behavior of granite: An experimental investigation, Eng. Fract. Mech. 250 (2021) 107758, https://doi.org/10.1016/J.ENGFRACMECH.2021.107758.
[25] J.A. Menéndez, A. Arenillas, B. Fidalgo, Y. Fernández, L. Zubizarreta, E.G. Calvo, J. M. Bermúdez, Microwave heating processes involving carbon materials, Fuel Process. Technol. 91 (2010) 1–8, https://doi.org/10.1016/J.FUPROC.2009.08.021.
[26] A.A. Metaxas, R.J. Meredith, Industrial Microwave Heating. No. 4 (1983) IET.
[27] W. Wei, Z. Shao, Y. Zhang, R. Qiao, J. Gao, Fundamentals and applications of microwave energy in rock and concrete processing – A review, Appl. Therm. Eng. 157 (2019) 113751, https://doi.org/10.1016/J.APPLTHERMALENG.2019.113751.
[28] J.H. Chen, D.T. Georgi, H.H. Liu, Electromagnetic thermal stimulation of shale reservoirs for petroleum production, J. Nat. Gas Sci. Eng. 59 (2018) 183–192, https://doi.org/10.1016/j.jngse.2018.08.029.
[29] P.K. Choudhury, Dielectric materials and applications, Dielectric Materials and Applications 102 (2019) 1–399, https://doi.org/10.1149/1.2430014.
[30] M. Al-Harahsheh, S.W. Kingman, Microwave-assisted leaching - A review, Hydrometall. 73 (3–4) (2004) 189–203, https://doi.org/10.1016/J.HYDROMET.2003.10.006.

[31] C.A. Pickles, Microwave heating behaviour of nickeliferous limonitic laterite ores, Mineral Engineering 17 (2004) 775–784, https://doi.org/10.1016/J.MINENG.2004.01.007.
[32] E.T. Thostenson, T.W. Chou, Microwave processing: fundamentals and applications, Compos. A Appl. Sci. Manuf. 30 (9) (1999) 1055–1071, https://doi.org/10.1016/S1359-835X(99)00020-2.
[33] I. Znamenácková, M. Lovás, M. Hájek, Š. Jakabský, Melting of andesite in a microwave oven, J. Min. Metall. Sect. b. 39 (2003) 549–557, https://doi.org/10.2298/JMMB0304549Z.
[34] J.R. Brandon, J. Samuels, W.R. Hodgkins, Microwave sintering of oxide ceramics, MRS Online Proceedings Library (OPL) 269 (1992) 237, https://doi.org/10.1557/PROC-269-237.
[35] S.L. McGill, J.W. Walkiewicz, G.A. Smyres, The effects of power level on the microwave heating of selected chemicals and minerals, MRS Online Proceedings Library (OPL) 124 (1988) 247, https://doi.org/10.1557/PROC-124-247.
[36] N. Dilissen, J. Vleugels, J. Vermeiren, B. García-Baños, J.R.S. Marín, J.M. Catalá-Civera, Temperature dependency of the dielectric properties of hydrated and ordinary Portland cement and their constituent phases at 2.45 GHz up to 1100 °C, Cem. Concr. Res. 165 (2023) 107067, https://doi.org/10.1016/J.CEMCONRES.2022.107067.
[37] X. Wu, J.R. Thomas, Experimental and theoretical study of microwave heating of thermal runaway materials mechanical engineering, Virgina Polytechnic institute and State University, Davis, W.A., Thomas, W.C., Scott, E.P., Clark, D.E, 2002. Doctoral dissertation,.
[38] K. Yan, B. An, Q. Yuan, Enabling hydrogen production from shale oil reservoirs: An experimental study using microwave-assisted catalytic heating, Society of Petroleum Engineers - SPE Energy Transition Symposium, ETS 2023 (2023) 22–23, https://doi.org/10.2118/215725-MS.
[39] J.H. Chen, D. Georgi, H.H. Liu, B. Lai Fracturing. Tight Rocks by Elevated Pore-Water Pressure Using Microwaving and Its Applications (2015) SPWLA pp. SPWLA-2015.
[40] J.H. Chen, S.M. Althaus, H.H. Liu, J. Zhang, G. Eppler, J.C. Duncan, Q. Sun, Electromagnetic-heating enhancement of source rock permeability for high recovery, Fuel 283 (2021) 118976, https://doi.org/10.1016/j.fuel.2020.118976.
[41] N.V. Seleznev, K. Fellah, J. Phillips, S.N. Zulkipli, B. Fournié, Matrix permittivity measurements for rock powders, SPE Reserv. Eval. Eng. 19 (2016) 214–225, https://doi.org/10.2118/170896-PA.
[42] R. Tempke, C. Wildfire, D. Shekhawat, T. Musho, Dielectric measurement of powdery materials using a coaxial transmission line, IET Sci. Meas. Technol. 14 (10) (2020) 972–978, https://doi.org/10.1049/iet-smt.2020.0055.
[43] M.R. Stuart, Dielectric constant of quartz as a function of frequency and temperature, J. Appl. Phys. 26 (1955) 1399–1404, https://doi.org/10.1063/1.1721922.
[44] G.A. Norton, The determination of quartz using differential scanning calorimetry, Thermochim Acta 237 (1994) 295–304, https://doi.org/10.1016/0040-6031(94)80187-8.
[45] H. Le Chatelier, Sur la dilatation du quartz, Bull. Minér. 13 (1890) 112–118, https://doi.org/10.3406/BULMI.1890.2156.
[46] X. Xie, Y. Cheng, K. Wu, B. Xiao, Study on α-β Quartz phase transition and its effect on dielectric properties, J. Appl. Phys. 111 (2012) 104116, https://doi.org/10.1063/1.4722217.
[47] R.C. Mackenzie, L.G. Berg, G. Berggren, Differential Thermal Analysis Application, 2, Academic Press, London, UK, 1972, pp. 135–142.
[48] J. Khinast, G.F. Krammer, C. Brunner, G. Staudinger, Decomposition of limestone: The influence of CO_2 and particle size on the reaction rate, Chem Eng Sci 51 (1996) 623–634, https://doi.org/10.1016/0009-2509(95)00302-9.
[49] M. Olszak-Humienik, M. Jablonski, Thermal behavior of natural dolomite, J. Therm. Anal. Calorim. 119 (2015) 2239–2248, https://doi.org/10.1007/S10973-014-4301-6.
[50] J. Gersten, V. Fainberg, G. Hetsroni, Y. Shindler, Kinetic study of the thermal decomposition of polypropylene, oil shale, and their mixture, Fuel 79 (13) (2000) 1679–1686, https://doi.org/10.1016/S0016-2361(00)00002-8.
[51] Y.L. Zheng, X.B. Zhao, Q.H. Zhao, J.C. Li, Q.B. Zhang, Dielectric properties of hard rock minerals and implications for microwave-assisted rock fracturing, Geomechanics and Geophysics for Geo-Energy and Geo-Resources 6 (2020) 1–17, https://doi.org/10.1007/S40948-020-00147-Z.
[52] X. Cong, S. Lu, Y. Gao, Y. Yao, M. Elchalakani, X. Shi, Effects of microwave, thermomechanical and chemical treatments of sewage sludge ash on its early-age behavior as supplementary cementitious material, J. Clean. Prod. 258 (2020) 120647.
[53] G. Wang, H. Wang, N. Zhang, In situ high temperature X-ray diffraction study of illite, Appl. Clay Sci. 146 (2017) 254–263, https://doi.org/10.1016/J.CLAY.2017.06.006.
[54] R.B. Ferguson, R.J. Traill, W.H. Taylor, The crystal structures of low-temperature and high-temperature albites, Acta Crystallogr. 11 (5) (1958) 331–348, https://doi.org/10.1107/S0365110X5800092X.
[55] J.D.F. Gerald, A.C. McLaren, The microstructures of microcline from some granitic rocks and pegmatites, Contrib. Miner. Petrol. 80 (1982) 219–229, https://doi.org/10.1007/BF00371351.
[56] X. Zhang, D.O. Hayward, D.M.P. Mingos, Apparent equilibrium shifts and hot-spot formation for catalytic reactions induced by microwave dielectric heating, Chem. Commun. 975–976 (1999), https://doi.org/10.1039/A901245A.
[57] A. Ramirez, J.L. Hueso, R. Mallada, J. Santamaria, In situ temperature measurements in microwave-heated gas-solid catalytic systems, Detection of Hot Spots and Solid-Fluid Temperature Gradients in the Ethylene Epoxidation Reaction, Chemical Engineering Journal 316 (2017) 50–60, https://doi.org/10.1016/j.cej.2017.01.077.